NANO LETTERS

pubs.acs.org/NanoLett

Letter

Large Damping-Like Spin–Orbit Torque in a 2D Conductive 1T-TaS_2 Monolayer

Sajid Husain, Xin Chen, Rahul Gupta, Nilamani Behera, Prabhat Kumar, Tomas Edvinsson, F. García-Sánchez, Rimantas Brucas, Sujeet Chaudhary, Biplab Sanyal, Peter Svedlindh,* and Ankit Kumar*

Cite This: *Nano Lett.* 2020, 20, 6372–6380

Read Online

ACCESS | Metrics & More | Article Recommendations | Supporting Information

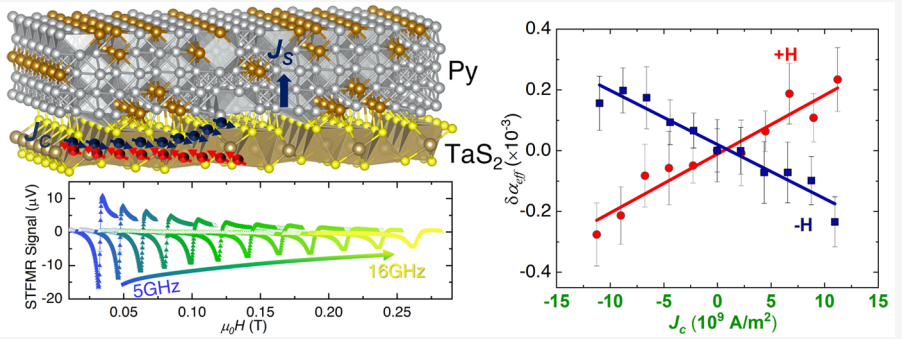

ABSTRACT: A damping-like spin-orbit torque (SOT) is a prerequisite for ultralow-power spin logic devices. Here, we report on the damping-like SOT in just one monolayer of the conducting transition-metal dichalcogenide (TMD) TaS_2 interfaced with a NiFe (Py) ferromagnetic layer. The charge-spin conversion efficiency is found to be 0.25 ± 0.03 in TaS_2(0.88)/Py(7), and the spin Hall conductivity $\left(14.9 \times 10^5 \frac{\hbar}{2e}\Omega^{-1}m^{-1}\right)$ is found to be superior to values reported for other TMDs. We also observed sizable field-like torque in this heterostructure. The origin of this large damping-like SOT can be found in the interfacial properties of the TaS_2/Py heterostructure, and the experimental findings are complemented by the results from density functional theory calculations. It is envisioned that the interplay between interfacial spin–orbit coupling and crystal symmetry yielding large damping-like SOT. The dominance of damping-like torque demonstrated in our study provides a promising path for designing the next-generation conducting TMD-based low-powered quantum memory devices.

KEYWORDS: *Transition-metal dichalcogenide, Damping-like torque, Spin-torque ferromagnetic resonance, Planar Hall effect*

Spin–orbit torques (SOTs) induced by spin currents are prerequisite to controlling the magnetization ($\boldsymbol{m}$) in next-generation nonvolatile three-terminal memory devices,[1−3] spin-torque nano-oscillators for microwave-assisted switching and neuromorphic computing.[4] SOT-based magnetic memories are considered to be more reliable by utilizing low energy induced switching of the magnetization in contrast to the low endurance and low speed of two-terminal spin-transfer torque (STT)-based random access memories. A spin current with spin polarization vector $\boldsymbol{\sigma}$ generated by the spin Hall effect (SHE) and/or the Rashba–Edelstein effect (REE) in the presence of high spin–orbit coupling (SOC) in a material may give rise to two types of SOTs, damping-like ($\boldsymbol{\tau}_{DL} = \boldsymbol{m} \times (\boldsymbol{m} \times \boldsymbol{\sigma})$) and field-like ($\boldsymbol{\tau}_{FL} = \boldsymbol{m} \times \boldsymbol{\sigma}$) torques, and have been reported for a number of heavy metals (HMs).[3,5−8] In contrast to STT devices where the spin polarization of the charge current passing through the free layer enforce the switching of the magnetization, the physical origin of SOTs is the transfer of spin and orbital angular momenta through exchange interaction process,[8] the latter via contributions mainly from different d orbitals.[9] The SOT in HMs is reported to be a bulk-like phenomenon, which requires the thickness of the HM layer to be larger than its spin diffusion length in order to produce appreciable torque.[10] However, it is difficult to control the crystallinity of the HM in the low thickness regime. Recently, very large SOT has been reported in topological insulators (TIs),[11,12] but the topological surface states are quenched if the TI is deposited next to a metallic ferromagnet

Received: May 6, 2020
Revised: August 4, 2020
Published: August 5, 2020

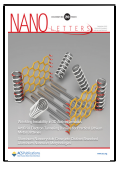

https://dx.doi.org/10.1021/acs.nanolett.0c01955
Nano Lett. 2020, 20, 6372–6380

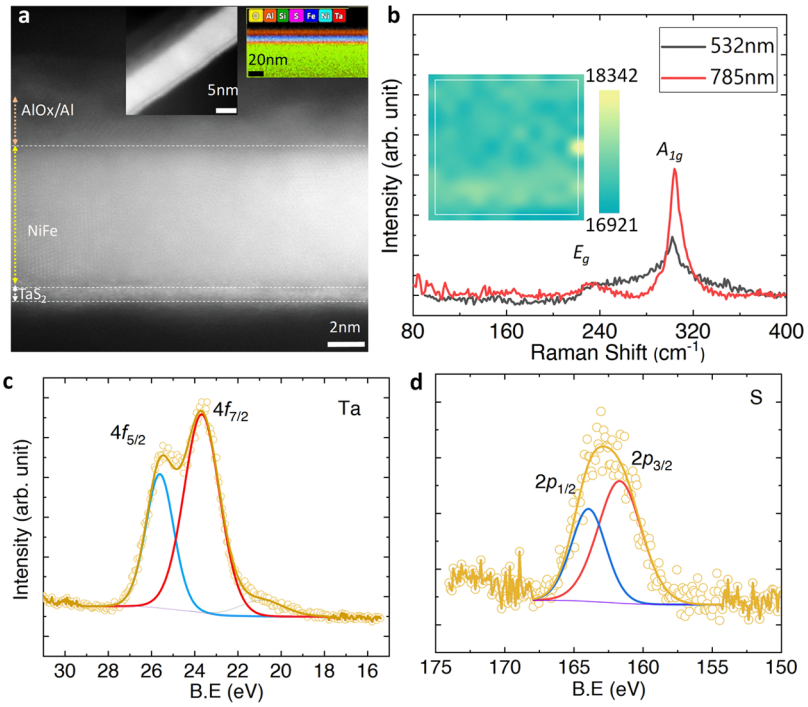

Figure 1. (a) High-resolution cross-sectional TEM image of the TaS_2(0.88)/Py(7)/Al(3) heterostructure. Insets: (left) low-magnification cross-sectional image; (right) elemental EDX mapping of the trilayer sample. (b) Raman spectra recorded using two lasers (532 and 785 nm) and mapping (10 × 10 μm^2) in an inset on single-layer TaS_2 using a 785 nm laser. (c, d) XPS spectra of Ta and S recorded on a single-layer TaS_2 sample.

and hence a ferromagnetic insulator is required to render high SOTs,[13] which implies industrial compatibility issues.[14]

To overcome the bulk-like effect in HMs, with perceived industrial compatibility, two-dimensional transition-metal dichalcogenides (2D-TMDs) were proposed a few years ago for spintronic applications.[15−18] By replacing the HMs with TMDs, one can anticipate two positive outcomes for spin devices. First, a pure spin current can be produced by just a monolayer thick TMD without any bulk-like effect. Second, being a layered material, it is possible to realize smooth surfaces with atomic-scale flatness, i.e., in the Ångström scale. Although there are few reports on the observation of SOTs in TMDs,[18,19] they are, however, encountered with the problem of a dominating field-like torque due to their semiconducting nature.[16,12] The SOC in TMDs/FM at the interface can also give Dzyaloshinkii−Moriya interaction (DMI),[20] which can generate chiral structures such as skyrmions. The surface quality of TMD exfoliated films grown by chemical vapor deposition is also compromised due to high roughness and strain.[21,22] TMD films produced in this way exhibit inhomogeneity and are thus not suitable for spintronic device applications. Thus, we are forced to face two challenges to realize the requirement of dominating damping-like torques in TMDs. One is to grow large-area TMDs directly on SiO_2 substrates and concomitantly to provide large damping-like torques by using conducting TMD/ferromagnet bilayers. Keeping in mind the growth problem of conducting TMDs, the 1T-tantalum-disulfide (TaS_2) system is yet to be explored, which can be easily fabricated by the sputtering technique along with the distinctive plasma sulphurization process. The prefix 1T in 1T-TaS_2 refers to 1 layer per trigonal (T) unit cell. Being conducting with high SOC,[23] the 1T-TaS_2 system also possesses exotic temperature-dependent properties, owing to several charge density wave (CDW) transitions,[24] thus contributing with the rich physics of CDWs to the field of SOTs. Previously, researchers have reported the growth of TaS_2 by various methods,[24−26] which is yet to be explored for spin−orbitronics.

Here, we report a dominating damping-like torque in conducting TaS_2/Py bilayer heterostructures. The high-quality large-area TaS_2 monolayers have been prepared by ion-beam sputtering combined with plasma-assisted sulfurization (see methods and materials for details in Supporting Information S1). The SOTs were measured by using spin-torque ferromagnetic resonance (ST-FMR) and angle-dependent planar Hall effect (PHE) measurements. First-principles calculations based on density functional theory envisage the possible source of the damping-like torque in the TaS_2/Py heterostructures. Micromagnetic simulations corroborate the experimental results.

Results. *Monolayer Characteristics.* Figure 1 shows the transmission electron microscopy (TEM) cross-sectional image of the TaS_2(1 ML)/Py(7)/Al(3) heterostructure. The thickness of the individual layers is found to be similar to the nominal ones. Notably, the thickness of the TaS_2 layer is found to be equivalent to one monolayer, which is around ∼0.88 nm. In the left inset, the large-scale TEM image shows a uniform film and sharp interface of TaS_2 in contact with the Py layer. Elemental mapping of the stack (inset) also supports the uniform growth of all layers in the stack (see Supporting Information, S14). It also confirms that our ferromagnet layer shows less affinity to sulfur because metals having a large affinity to sulfur can degrade the 2D characteristics of TMDs.[27] Figure 1b shows the room-temperature Raman spectra recorded on a single-layer TaS_2 film using two different lasers. Strong fundamental peaks are observed at 305 and 231 cm^{-1},

https://dx.doi.org/10.1021/acs.nanolett.0c01955
Nano Lett. 2020, 20, 6372−6380

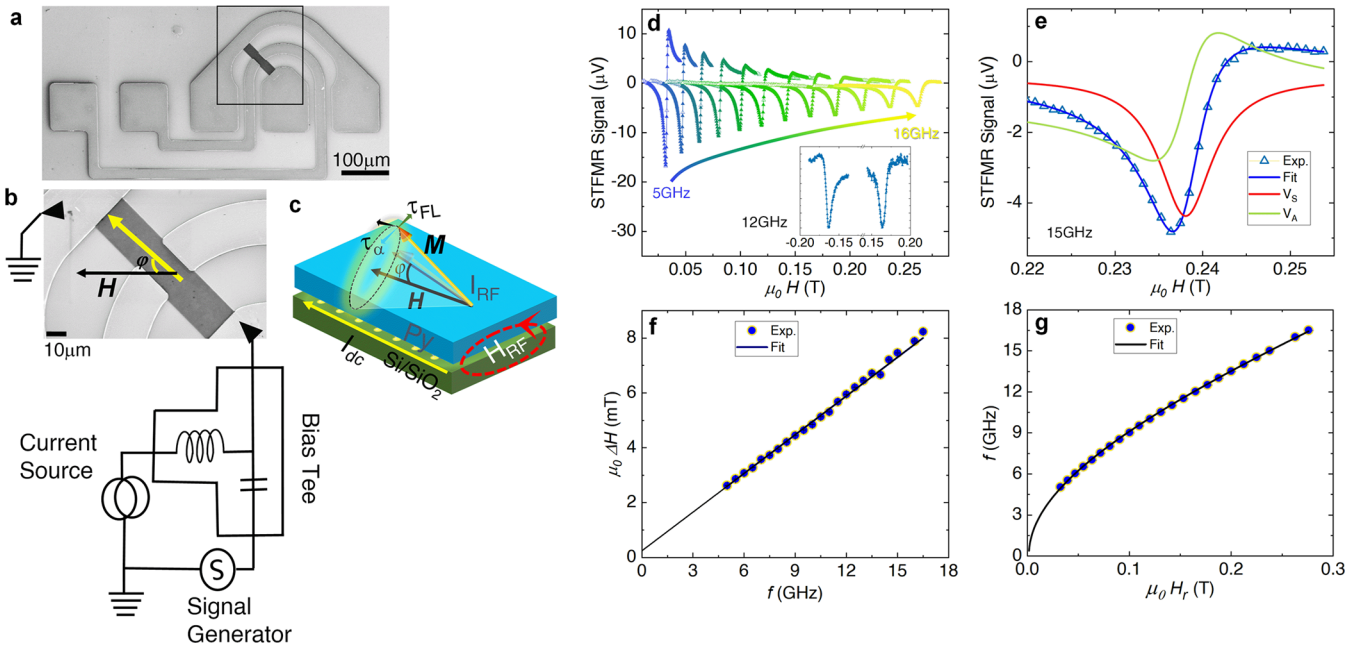

Figure 2. (a) Scanning electron microscopic (SEM) image of the $TaS_2(0.88)$/Py(7) device. (b) High-magnification SEM image (area indicated by a square in panel a showing the ST-FMR measurement circuit). (c) Layer schematic shown with torques acting on the magnetization. (d) ST-FMR spectra recorded at various frequencies in the range of 5−16 GHz. Inset, ST-FMR spectra at 12 GHz recorded in opposite magnetic field directions. (e) ST-FMR spectrum (recorded at 15 GHz) fitted separately with symmetric and antisymmetric Lorentzian unctions. (f, g) Line width and resonance field versus frequency plots, respectively.

corresponding to the 1T-TaS_2 phase.[28] The uniformity of the film can be seen in the Raman mapping as recorded around the most intense Raman peak (shown in the inset). Elemental analysis has been performed by X-ray photoelectron spectroscopy (XPS) as presented in Figure 1c,d for Ta and S, respectively. Observed peaks are deconvoluted into the two spin−orbit split peaks, which confirms the TaS_2 formation without residual phases.[29,30] We also observed a finite shift around 1.5 ± 0.9 eV for the Ta($4f_{7/2}$) orbital peak position in TaS_2 in comparison to the metal Ta,[31] which indicates a large spin-orbit splitting in TaS_2. Further, surface topography and step height scans were also recorded using atomic force microscopy and confirm the monolayer thickness and the smooth interface with Ångström scale flatness of the TaS_2 layer (see Supporting Information, S4).

ST-FMR Measurements. The magnitude of the SOT efficiency governed by the spin-torque efficiency (θ_S) was measured using ST-FMR. The applied field makes an angle of 45° with respect to the current as shown in Figure 2a (scanning electron microscopic (SEM) image of the device). An SEM image with the measurement circuit is shown in Figure 2b. A schematic of the torques acting on the magnetization due to the microwave current I_{RF} is shown in Figure 2c. The ST-FMR measurements were performed in a field-sweep mode in the frequency range of 5−16 GHz. We have used a lock-in detection technique with an I_{RF} current frequency modulation of 1000 Hz at 9 dB microwave power (see Supporting Information, S7).

The rf current generates an Oersted field as well as spin−orbit torques in the presence of the magnetic field and acts as torques on the magnetization. The I_{RF}-induced torque acting on the Py layer generates a sustained precession of the magnetization, which mixes with the anisotropic magnetoresistance and spin Hall magnetoresistance creating a dc-mixing voltage V_{mix}. This rectified mixing voltage provides the information on the material parameters and torques acting on the magnetization, which is written as[32] $V_{mix} = V_0(Sfs + Afa)$. Here, V_0 is the amplitude of the mixing voltage, and fs and fa are symmetric and antisymmetric Lorentzian functions, respectively. $S = \hbar J_{rf}/2e\mu_0 M_S t_{Py}$ and $A = \mu_0 H_{RF}\sqrt{1 + \frac{M_{eff}}{H_r}}$ are symmetric and antisymmetric weight factors, respectively, where μ_0, e, t_{Py}, J_{rf}, M_S, H_{RF}, H_r, and M_{eff} are the magnetic permeability in free space, electronic charge, thickness of ferromagnet layer, rf-current density, saturation magnetization, microwave field, resonance field, and effective magnetization, respectively.

Figure 2d shows the ST-FMR spectra together with fits using the equation for V_{mix}, which give the line-shape parameters. The ST-FMR spectra for positive and negative magnetic field scans are shown in the inset (at 12 GHz). It is to be noted that the peak changes its sign on changing the direction of the external magnetic field, indicating a damping-like torque τ_{DL} and ruling out the possibility of a dominating Oersted field generated torque (τ_{FL}). The symmetric and antisymmetric amplitudes have been separately fitted to the spectra; an example for the spectrum recorded at 15 GHz is shown in Figure 2e. The effective damping (α_{eff}) of the $TaS_2(0.88)$/Py(7) bilayer is evaluated by fitting the $\mu_0\Delta H$ versus f data (as shown in Figure 2f) using the equation, $\mu_0\Delta H = \mu_0\Delta H_0 + 2\alpha_{eff}\omega/\gamma$, where $\mu_0\Delta H_0$ is the line width contribution from inhomogeneity in the magnetic film, ω (=$2\pi f$) is the microwave frequency, and $\gamma/2\pi$ (28.8 GHz/T) is the magnetogyric ratio. From the fitting, the values of effective damping are found to be 0.0067 ± 0.0007. The inhomogeneous line width is found to be 0.20 ± 0.02 mT, which is quite small and indicative of a smooth and clean interface of the Py/TaS_2 heterostructure. Further, $\mu_0 M_{eff}$ and the anisotropy field ($\mu_0 H_K$) values have been calculated by fitting the f versus $\mu_0 H_r$ data to the Kittel equation, $f = \mu_0\gamma/2\pi[(H_r + H_K)(H_r + H_K +$

https://dx.doi.org/10.1021/acs.nanolett.0c01955
Nano Lett. 2020, 20, 6372−6380

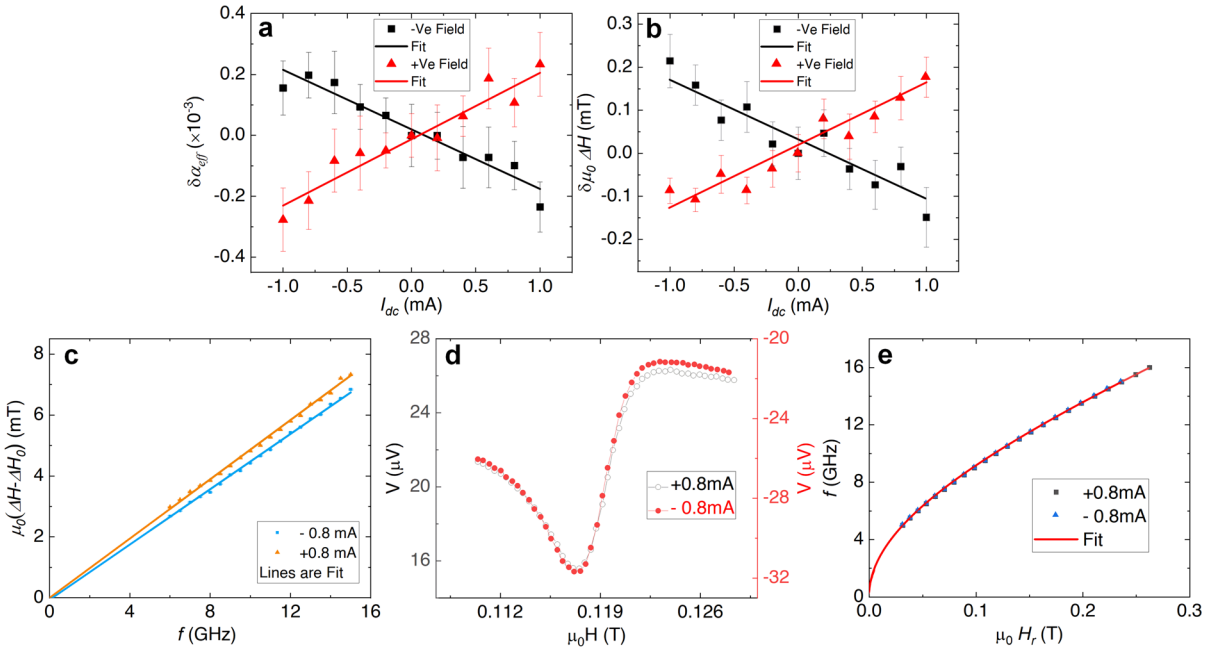

Figure 3. (a) dc-induced changes of effective damping in the TaS_2(0.88)/Py(7) bilayer for positive and negative field directions. (b) dc-induced line width changes for positive and negative magnetic fields. (c) Line width versus frequency. (d) ST-FMR spectra recorded at 10 GHz and (e) frequency versus resonance field measured at +0.8 mA and −0.8 mA dc applied to the device in a positive magnetic field.

M_{eff})]$^{1/2}$, yielding 0.902 ± 0.004 T and 1.8 ± 0.4 mT, respectively. The values of $\mu_0 M_s$ of TaS_2(0.88)/Py(7) are measured using a QD-MPMS setup and found to be 1.00 ± 0.02 T (see Supporting Information, S5), which is consistent with the $\mu_0 M_{eff}$ value extracted from the ST-FMR results considering the out-of-plane anisotropy field contribution to the effective magnetization.

From the line-shape parameters, the value of the spin-torque efficiency θ_S is evaluated using the standard line-shape analysis method[33] and found to be 0.023 ± 0.01. However, in this method, it is assumed that the symmetric component is purely from a damping-like torque, disregarding a possible contribution from spin pumping due to the inverse spin Hall effect (ISHE) and can, therefore, yield erroneous values for the SOT efficiency.[34−36] Concomitantly, the antisymmetric component is considered as an Oersted field generated torque component, but it is again a naive approximation.[35] Moreover, the line-shape analysis also shows a frequency dependency,[33] which may lead to the wrong estimation of the effective spin-torque efficiency. Hence, to determine a reliable value of the effective spin-torque efficiency and evidence of damping-like torque, we use the so-called damping modulation scheme by applying a dc during the ST-FMR measurement, where spin pumping due to the ISHE and field-like contributions are insignificant.

Current Induced Modulation/Changes of Effective Damping in the TaS_2(0.88)/Py(7) Device. In this method, the dc-induced nonequilibrium spin accumulation at the interface, resulting due to the SHE in TaS_2, acts as a torque on the Py magnetization, resulting in a change of the effective damping as described by[33,35]

$$\delta\alpha_{eff} = \alpha_{eff}(I_{dc} \neq 0) - \alpha_{eff}(I_{dc} = 0) = \frac{\sin\varphi}{(H_r + 0.5M_{eff})\mu_0 M_S t_{Py}} \frac{\hbar}{2e} J_{S,dc}$$

The effective spin-torque efficiency using the dc-induced change of the damping is defined as the ratio of spin to charge current density: $\theta_S^{\alpha} = \frac{J_{S,dc}}{J_{C,dc}}$. Here, $J_{C,dc} = \frac{I_{dc}}{A_d} \frac{R_{Py}}{R_{Py} + R_{TaS_2}}$, where R_{Py}, R_{TaS_2}, and A_d are the resistances of permalloy and TaS_2, respectively, and the cross-sectional area of the device. φ is the angle between the magnetization and the applied field, which is 45° in our case. Figure 3a shows the change/modulation of effective damping as a function of the dc (I_{dc}). For comparison, the $\delta\alpha_{eff}$ values are plotted for the two directions of the magnetic field scan. The corresponding changes of $\mu_0\Delta H$ with dc, i.e., $\delta\mu_0\Delta H$, are shown in Figure 3b. The slopes of the $\delta\alpha_{eff}$ versus I_{dc} curves for the two field directions are almost equal, which confirm that the damping-like torque acting on the magnetization in our TaS_2/Py bilayer is due to the SHE generated spin current. The damping values are reversed on current polarity reversal. This reversal is also observed when reversing the magnetic field direction. Therefore, the spin Seebeck and anomalous Nernst effect induced modulation of the damping can be ruled out in our measurements. The slope of the change in α_{eff} with dc ($\frac{\delta\alpha_{eff}}{\delta I_{dc}}$) is 2.17 ± 0.21 × 10^{-4}/mA and 1.95 ± 0.17 × 10^{-4}/mA for positive and negative applied fields, respectively. Using the measured resistances of Py (225 Ω) TaS_2 (952 Ω) (see Supporting Information, S8) in the equation for $J_{C,dc}$, the θ_S^{α} value is found to be 0.25 ± 0.03. Within the experimental uncertainty, the values of the spin-torque efficiency are the same for both positive and negative field scans. The obtained value is better than the values reported for other TMDs.[37,20,38] The intercept with the current axis is known as the critical current density for auto-oscillations and estimated to be 5.13 × 10^{10} A/m.[2] ST-FMR measurements were also performed on a controlled Ta(0.9)/Py(7) device, which shows a weak signal-to-noise ratio (see Figure S11). We further measured the efficiency of various Py thicknesses with a fixed TaS_2 layer (see Supporting Information, S10b). The spin Hall conductivity (SHC) ($\sigma_S = \sigma_{dc} \times \theta_S^{\alpha}$) is found to be 14.9 × 10^5 $\frac{\hbar}{2e}$ (Ω−m)$^{-1}$, using σ_{dc} = 5.9 × 10^6 (Ω−m)$^{-1}$ of TaS_2 and θ_S^{α} = 0.25. The SHC value is ∼10 times smaller than the value reported for the TI $Bi_{0.9}Sb_{0.1}$/

https://dx.doi.org/10.1021/acs.nanolett.0c01955
Nano Lett. 2020, 20, 6372−6380

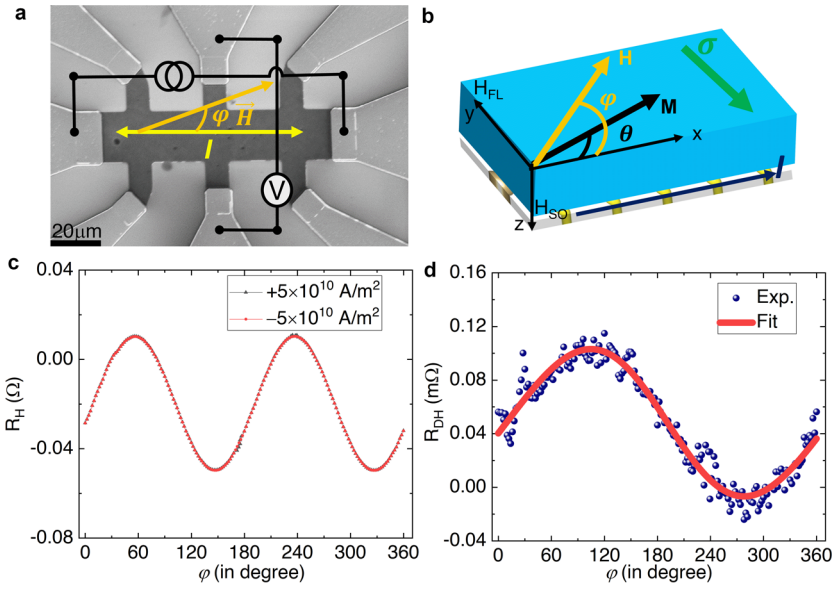

Figure 4. (a) SEM image of the TaS_2(0.88)/Py(7) Hall bar (100 × 20 μm^2) device together with a schematic of the circuit used for planar Hall effect measurements. The angle φ (θ) is the in-plane angle between the magnetic field (magnetization) and the current direction in the device. (b) Vector components of the applied field H, magnetization, and the fields generated by SOTs. (c) Planar Hall effect signal recorded for two directions of the dc (magnitude = 5 × 10^{10} A/m^2) in the presence of an in-plane magnetic field of 0.4 T. (d) Plot of the Hall resistance difference observed for two current directions versus angle φ.

MnGa,[12] 100 times larger than for the field-like torque-dominated semiconducting TMDs $MoSe_2$ and WS_2,[19] conducting TMD $NbSe_2$[17] and comparable to that of the $Pd_{1-x}Pt_x$ alloy.[39] TIs suffer from issues related to industrial compatibility,[14] while HMs and alloys have limitations with respect to the spin diffusion length due to the spin relaxation being controlled by the Elliot−Yafet[40] and D'yakonov−Perel'[41] scattering mechanisms. The conducting TMD 1T-TaS_2 investigated in this work is an industrial compatible material and is easy to fabricate for SOT devices and therefore avoid such limitations. Moreover, 1T-TaS_2 provides rich physics due to its inherent property of CDW fluctuations, where electrons collectively may carry a charge current in a highly correlated fashion.

The dc-induced changes of the effective damping can also be seen in the $\mu_0\Delta H$ versus f results shown in Figure 3c for positive and negative direct currents. The current distribution in the heterostructure was evaluated, and it was found that 19% of the current is flowing through the TaS_2(0.88) layer (see Supporting Information, S8). Consequently, the Oersted field $\mu_0 H_{Oe}$ in the TaS_2(0.88) layer is found to be ∼0.012 mT/mA, which is very small, and it is, therefore, concluded that the field-like torque contribution generated by dc passing through the TaS_2 layer can be neglected. The ST-FMR spectra and resonance field plots shown for two currents in Figure 3d,e, respectively, show no change during a current polarity reversal, which is indicative of negligible field-like torque contributions. However, a small field-like torque contribution can arise from the unavoidable interface symmetry breaking,[42,43] which is discussed in Supporting Information, S10a.

We validate the dc-induced damping-like torque in the TaS_2(0.88)/Py(7) device by means of magnetization in the in-plane field scan in two opposite current directions, which yield the opposite hysteresis formation, discussed in Supporting Information, S12. The magnetization switching indicates the presence of dominating damping-like torque in TaS_2(0.88)/Py(7). The Hall voltage hysteresis was also recorded using a Hall bar structure as is shown in Supporting Information, S11d. Further, using micromagnetic simulations, the switching of the in-plane magnetization for different current amplitudes has also been studied (see Supporting Information, Figure S13).

Angle-Dependent Planar Hall Effect (PHE) for SOTs. Planar Hall effect (PHE) measurements have received much attention for characterizing the SOTs in the in-plane magnetized systems.[44−46] Figure 4a shows a scanning electron microscope (SEM) image of the Hall device used for PHE measurements. A schematic of the measurement circuit has been added to the image. In the planar Hall measurement, the sample is rotated 360° at fixed dc. The vector representation of the PHE is shown in Figure 4b, where φ is the angle between the current direction and the applied field, and θ is the angle between the current direction and the magnetization vector. The theoretical background of the PHE is discussed in Supporting Information, S11a. Figure 4c shows the PHE signal (R_H) versus φ recorded for two direct currents of the same magnitude but of opposite polarity. A magnetic field of 0.4 T was used for the measurements, which was enough for suppressing the field-like torque contribution. The PHE measured at different magnetic fields and currents are discussed in the Supporting Information, S11a. The difference between the curves (R_{DH}) is plotted as a function of φ in Figure 4d, which embraces the dominance of the damping-like torque. The R_{DH} versus φ curve was fitted using eq S12 with H_{FL} and H_{SO} as fitting parameters. The H_{SO} field determines the amount of damping-like torque acting on the ferromagnetic layer. The value is found to be 1 Oe per 10^{10} A/m,[2] from which the spin-torque efficiency (ζ_S) has been obtained by using the expression, $\zeta_S = \frac{2e\mu_0 M_s t_{Py}}{\hbar}\frac{H_{SO}}{J_{c,dc}}$. The field-like contribution H_{FL} has been found to be negligibly small. The dc density J_c can be calculated by considering the dimensions of the device and the conductivity values at a dc value of 4.5 mA, yielding a dc density of 5 × 10^{10} A/m.[2] Using the thickness

https://dx.doi.org/10.1021/acs.nanolett.0c01955
Nano Lett. 2020, 20, 6372−6380

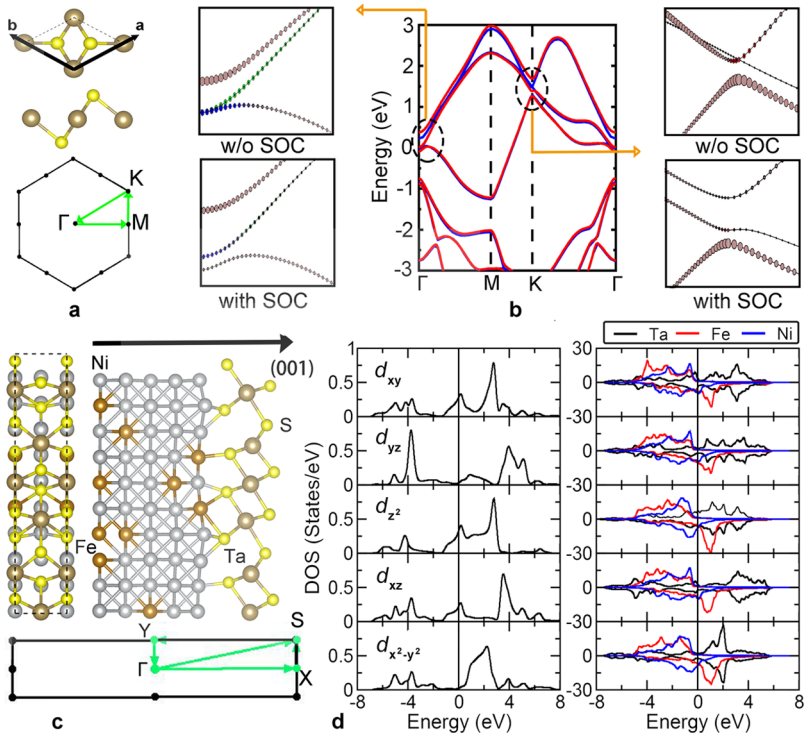

Figure 5. (a) Unit cell and Brillouin zone of pristine TaS_2. Both top and side views of the hexagonal unit cell are shown. (b) Band structure of pristine TaS_2 with and without spin−orbit coupling (SOC) (middle panel), expanded view of a part of the band structure (encircled) at the Γ point without and with SOC (left panel) and the same but at the K point (right panel). (c) Top and side views of the unit cell of TaS_2/Py illustrating the optimized geometry. In the lower panel, the BZ is shown. (d) (left) Projected densities of states (DOSs) for different d orbital symmetries of Ta for pristine TaS_2 and (right) spin-polarized projected DOSs for the TaS_2/Py system, where the d orbitals of Ta, Fe, and Ni are shown.

and saturation magnetization, ζ_S is found to be 0.19 ± 0.01, which is comparable to the value obtained using the ST-FMR analysis. We have also measured the Py thickness-dependent efficiency (see Supporting Information, S11b). For comparison, we have measured the angle-dependent PHE on the Ta(0.9)/Py(7) reference sample, which shows a very weak signal-to-noise ratio (see Supporting Information, S11c). Therefore, it is confirmed without a doubt that a monolayer of 1T-TaS_2 produces a damping-like torque acting on the Py magnetization.

Discussion. It is to be pointed that the possibility of a finite field-like torque contribution is not ruled out (see Figure S10a) in this work, which is reasonable and cannot be disentangled in SOT-based systems.[42,43,47] There has been no clear evaluation of the critical current density and spin-torque efficiency in previously reported results for TMD/FM heterostructures.[17−19] The quantitative estimation of the SHC and auto-oscillations current density in our TaS_2/Py hold valuable information for several spintronic applications. Evidently, the interface of our TaS_2/Py bilayer, as confirmed by cross-sectional TEM and supported by parameters extracted from X-ray reflectivity measurements, is clean in contrast to other works using exfoliated sheets and nonuniform growth where extrinsic contributions from strain and defect-related issues[17,48,38] reduce the charge-spin conversion efficiency. First-principles calculations based on the density functional theory (DFT) reveal the role of SOC for lifting the degeneracy in the band structure of TaS_2/Py. Figure 5 shows the energy band structures without and with the inclusion of SOC for both pristine TaS_2 and TaS_2/Py systems. A detailed discussion of the structural and electronic properties is presented in Supporting Information, S2. For pristine TaS_2, the effects of SOC are clearly observed at Γ and K points (see the expanded views). Specifically, at the Γ point, the degenerate d_{xz} and d_{yz} bands are split due to SOC. It should be noted that this degeneracy is already lifted by the lower symmetry present at the interface between TaS_2 and Py due to the distorted atomic structures. On top of that, further splitting occurs due to the presence of SOC. Therefore, one can conclude that a sizable redistribution of band structure and hence the splitting of states due to the interface occurs, which becomes responsible for prominent damping-like torque. Moreover, a low-symmetry-induced out-of-plane unconventional torque,[49] which mimics the out-of-plane Rashba-like or field like torque, can also be present in this heterostructure (see Supporting Information, S10a). To highlight the contribution from different d orbitals, we show in Figure 5d the orbital projected DOSs of Ta in pristine TaS_2 and also for the TaS_2/Py bilayer. Moreover, the projected DOSs of d orbitals of Fe and Ni in Py are shown to reveal features of hybridization. As our energy range of interest is in the vicinity of the Fermi level, we will consider the electronic states within that energy range. It is observed that in the pristine material, d_{xy}, d_{z^2}, and d_{xz} are the orbitals of interest. However, for the bilayer, the d_{z^2} orbital for both spin channels is quite prominent at the Fermi level and its vicinity. Moreover, for the spin-down channel, hybridization between the d_{z^2} orbitals of Ta and Ni is seen for the spin-down channel.

In conclusion, the damping-like spin-torque efficiency has been carefully investigated in the one monolayer of TaS_2 using ST-FMR and PHE measurements. Employing effective damping modulation or changes with dc, the effective spin-torque

https://dx.doi.org/10.1021/acs.nanolett.0c01955
Nano Lett. 2020, 20, 6372−6380

efficiency is found to be 0.25 ± 0.03 in TaS_2 (1 ML)/Py(7). Angle-dependent PHE measurements verify the spin-torque efficiency and clearly reveal the dominance of damping-like torque in our 1 ML TaS_2/Py bilayers. Further, the microscopic origin of the observed dominance of damping-like torque has been substantiated by DFT calculations. The observation of a dominating damping-like torque in just one monolayer provides a path for how to use TaS_2 in future spin−orbitronic devices.

■ ASSOCIATED CONTENT

Supporting Information

The Supporting Information is available free of charge at https://pubs.acs.org/doi/10.1021/acs.nanolett.0c01955.

Full growth and characterization details, density functional theory, crystal structure and thickness analysis, atomic force microscopy, magnetization measurements, angular dependent FMR for in-plane anisotropy measurement, power calibration for ST-FMR measurement, resistivity measurement and current distribution, RF-current measurement in TaS_2(0.88)/Py(7) device, field-like contributions in TaS_2(1 ML)/Py(t_{Py}), Py thickness-dependent damping modulation using ST-FMR, current modulation in Ta(0.9)/Py(7), planar Hall effect (PHE) for spin-orbit torques, Py thickness-dependent SOT using PHE, comparison between Py, Ta/Py, and TaS_2/Py, magnetization switching in the presence of in-plane field at constant dc, micromagnetic modeling, and elemental mapping using STEM (PDF)

■ AUTHOR INFORMATION

Corresponding Authors

Peter Svedlindh − *Department of Materials Science, Uppsala University, SE-751 03 Uppsala, Sweden*; Email: Peter.svedlindh@angstrom.uu.se

Ankit Kumar − *Department of Materials Science, Uppsala University, SE-751 03 Uppsala, Sweden*; orcid.org/0000-0002-1168-3287; Email: chainutyagi@gmail.com

Authors

Sajid Husain − *Department of Materials Science, Uppsala University, SE-751 03 Uppsala, Sweden*; orcid.org/0000-0002-2518-5430

Xin Chen − *Department of Physics and Astronomy, Materials Theory, Uppsala University, SE-751 20 Uppsala, Sweden*

Rahul Gupta − *Department of Materials Science, Uppsala University, SE-751 03 Uppsala, Sweden*; orcid.org/0000-0001-6523-3161

Nilamani Behera − *Department of Materials Science, Uppsala University, SE-751 03 Uppsala, Sweden*

Prabhat Kumar − *Department of Thin Films and Nanostructures, Institute of Physics of the Czech Academy of Sciences, 162 00 Prague, Czech Republic*; orcid.org/0000-0001-5383-949X

Tomas Edvinsson − *Department of Materials Science, Uppsala University, SE-751 03 Uppsala, Sweden*; orcid.org/0000-0003-2759-7356

F. García-Sánchez − *Departamento de Física Aplicada, University of Salamanca, 37008 Salamanca, Spain*; orcid.org/0000-0002-3655-4836

Rimantas Brucas − *Department of Materials Science, Uppsala University, SE-751 03 Uppsala, Sweden*

Sujeet Chaudhary − *Thin Film Laboratory, Department of Physics, Indian Institute of Technology Delhi, New Delhi 110016, India*; orcid.org/0000-0002-0535-6132

Biplab Sanyal − *Department of Physics and Astronomy, Materials Theory, Uppsala University, SE-751 20 Uppsala, Sweden*

Complete contact information is available at: https://pubs.acs.org/10.1021/acs.nanolett.0c01955

Notes

The authors declare no competing financial interest.

■ ACKNOWLEDGMENTS

The Swedish Research Council (VR) supports this work (2017-03799). Authors thank Seda Ullusoy for SEM imaging. We thank Cheuk-Wai Tai for providing cross-sectional TEM measurements. D. M. Polishchuk and V. Korenivski, Nanostructure Physics, Royal Institute of Technology, Stockholm, Sweden are gratefully acknowledged for providing the Ta/Py reference sample.

■ REFERENCES

(1) Emori, S.; Bauer, U.; Ahn, S.-M.; Martinez, E.; Beach, G. S. D. Current-Driven Dynamics of Chiral Ferromagnetic Domain Walls. *Nat. Mater.* **2013**, *12*, 611−616.

(2) Safeer, C. K.; Jué, E.; Lopez, A.; Buda-Prejbeanu, L.; Auffret, S.; Pizzini, S.; Boulle, O.; Miron, I. M.; Gaudin, G. Spin-Orbit Torque Magnetization Switching Controlled by Geometry. *Nat. Nanotechnol.* **2016**, *11* (2), 143−146.

(3) Garello, K.; Miron, I. M.; Avci, C. O.; Freimuth, F.; Mokrousov, Y.; Blügel, S.; Auffret, S.; Boulle, O.; Gaudin, G.; Gambardella, P. Symmetry and Magnitude of Spin-Orbit Torques in Ferromagnetic Heterostructures. *Nat. Nanotechnol.* **2013**, *8* (8), 587−593.

(4) Chen, T.; Dumas, R. K.; Eklund, A.; Muduli, P. K.; Houshang, A.; Awad, A. A.; Dürrenfeld, P.; Malm, B. G.; Rusu, A.; Akerman, J. Spin-Torque and Spin-Hall Nano-Oscillators. *Proc. IEEE* **2016**, *104* (10), 1919−1945.

(5) Kim, J.; Sinha, J.; Hayashi, M.; Yamanouchi, M.; Fukami, S.; Suzuki, T.; Mitani, S.; Ohno, H. Layer Thickness Dependence of the Current-Induced Effective Field Vector in Ta|CoFeB|MgO. *Nat. Mater.* **2013**, *12* (3), 240−245.

(6) Zhang, W.; Han, W.; Jiang, X.; Yang, S.-H.; S. P. Parkin, S. Role of Transparency of Platinum−Ferromagnet Interfaces in Determining the Intrinsic Magnitude of the Spin Hall Effect. *Nat. Phys.* **2015**, *11* (6), 496−502.

(7) Kurebayashi, H.; Sinova, J.; Fang, D.; Irvine, A. C.; Skinner, T. D.; Wunderlich, J.; Novák, V.; Campion, R. P.; Gallagher, B. L.; Vehstedt, E. K.; et al. An Antidamping Spin-Orbit Torque Originating from the Berry Curvature. *Nat. Nanotechnol.* **2014**, *9* (3), 211−217.

(8) Manchon, A.; Železný, J.; Miron, I. M.; Jungwirth, T.; Sinova, J.; Thiaville, A.; Garello, K.; Gambardella, P. Current-Induced Spin-Orbit Torques in Ferromagnetic and Antiferromagnetic Systems. *Rev. Mod. Phys.* **2019**, *91*, 035004.

(9) Mahfouzi, F.; Mishra, R.; Chang, P. H.; Yang, H.; Kioussis, N. Microscopic Origin of Spin-Orbit Torque in Ferromagnetic Heterostructures: A First-Principles Approach. *Phys. Rev. B: Condens. Matter Mater. Phys.* **2020**, *101* (6), No. 060405(R).

(10) Berger, A. J.; Edwards, E. R. J.; Nembach, H. T.; Karis, O.; Weiler, M.; Silva, T. J. Determination of the Spin Hall Effect and the Spin Diffusion Length of Pt from Self-Consistent Fitting of Damping Enhancement and Inverse Spin-Orbit Torque Measurements. *Phys. Rev. B: Condens. Matter Mater. Phys.* **2018**, *98* (2), 024402.

(11) Mellnik, A. R.; Lee, J. S.; Richardella, A.; Grab, J. L.; Mintun, P. J.; Fischer, M. H.; Vaezi, A.; Manchon, A.; Kim, E. A.; Samarth, N.; et al. Spin-Transfer Torque Generated by a Topological Insulator. *Nature* **2014**, *511* (7510), 449−451.

(12) Khang, N. H. D.; Ueda, Y.; Hai, P. N. A Conductive Topological Insulator with Large Spin Hall Effect for Ultralow Power Spin−Orbit Torque Switching. *Nat. Mater.* **2018**, *17* (9), 808−813.
(13) Li, P.; Kally, J.; Zhang, S. S. L.; Pillsbury, T.; Ding, J.; Csaba, G.; Ding, J.; Jiang, J. S.; Liu, Y.; Sinclair, R.; et al. Magnetization Switching Using Topological Surface States. *Sci. Adv.* **2019**, *5* (8), No. eaaw3415.
(14) Pai, C. F. Switching by Topological Insulators. *Nat. Mater.* **2018**, *17* (9), 755−757.
(15) Feng, Y. P.; Shen, L.; Yang, M.; Wang, A.; Zeng, M.; Wu, Q.; Chintalapati, S.; Chang, C. R. Prospects of Spintronics Based on 2D Materials. *Wiley Interdiscip. Rev. Comput. Mol. Sci.* **2017**, *7*, e1313.
(16) Husain, S.; Kumar, A.; Kumar, P.; Kumar, A.; Barwal, V.; Behera, N.; Choudhary, S.; Svedlindh, P.; Chaudhary, S. Spin Pumping in the Heusler Alloy C O2FeAl/Mo S2 Heterostructure: Ferromagnetic Resonance Experiment and Theory. *Phys. Rev. B: Condens. Matter Mater. Phys.* **2018**, *98* (18), No. 180404(R).
(17) Guimarães, M. H. D.; Stiehl, G. M.; MacNeill, D.; Reynolds, N. D.; Ralph, D. C. Spin-Orbit Torques in NbSe2/Permalloy Bilayers. *Nano Lett.* **2018**, *18* (2), 1311−1316.
(18) Lv, W.; Jia, Z.; Wang, B.; Lu, Y.; Luo, X.; Zhang, B.; Zeng, Z.; Liu, Z. Electric-Field Control of Spin-Orbit Torques in WS2/Permalloy Bilayers. *ACS Appl. Mater. Interfaces* **2018**, *10* (3), 2843−2849.
(19) Shao, Q.; Yu, G.; Lan, Y. W.; Shi, Y.; Li, M. Y.; Zheng, C.; Zhu, X.; Li, L. J.; Amiri, P. K.; Wang, K. L. Strong Rashba-Edelstein Effect-Induced Spin-Orbit Torques in Monolayer Transition Metal Dichalcogenide/Ferromagnet Bilayers. *Nano Lett.* **2016**, *16* (12), 7514−7520.
(20) Shi, S.; Liang, S.; Zhu, Z.; Cai, K.; Pollard, S. D.; Wang, Y.; Wang, J.; Wang, Q.; He, P.; Yu, J.; et al. All-Electric Magnetization Switching and Dzyaloshinskii−Moriya Interaction in WTe2/Ferromagnet Heterostructures. *Nat. Nanotechnol.* **2019**, *14* (10), 945−949.
(21) You, J.; Hossain, M. D.; Luo, Z. Synthesis of 2D Transition Metal Dichalcogenides by Chemical Vapor Deposition with Controlled Layer Number and Morphology. *Nano Converg* **2018**, *5* (1), 26.
(22) Yun, S. J.; Chae, S. H.; Kim, H.; Park, J. C.; Park, J. H.; Han, G. H.; Lee, J. S.; Kim, S. M.; Oh, H. M.; Seok, J.; et al. Synthesis of Centimeter-Scale Monolayer Tungsten Disulfide Film on Gold Foils. *ACS Nano* **2015**, *9* (5), 5510−5519.
(23) Sanders, C. E.; Dendzik, M.; Ngankeu, A. S.; Eich, A.; Bruix, A.; Bianchi, M.; Miwa, J. A.; Hammer, B.; Khajetoorians, A. A.; Hofmann, P. Crystalline and Electronic Structure of Single-Layer TaS2. *Phys. Rev. B: Condens. Matter Mater. Phys.* **2016**, *94* (8), 1−5.
(24) Wang, X.; Liu, H.; Wu, J.; Lin, J.; He, W.; Wang, H.; Shi, X.; Suenaga, K.; Xie, L. Chemical Growth of 1T-TaS 2 Monolayer and Thin Films: Robust Charge Density Wave Transitions and High Bolometric Responsivity. *Adv. Mater.* **2018**, *30* (38), 1800074.
(25) Navarro-Moratalla, E.; Island, J. O.; Manãs-Valero, S.; Pinilla-Cienfuegos, E.; Castellanos-Gomez, A.; Quereda, J.; Rubio-Bollinger, G.; Chirolli, L.; Silva-Guillén, J. A.; Agraït, N.; et al. Enhanced Superconductivity in Atomically Thin TaS 2. *Nat. Commun.* **2016**, *7*, 11043.
(26) Fu, W.; Chen, Y.; Lin, J.; Wang, X.; Zeng, Q.; Zhou, J.; Zheng, L.; Wang, H.; He, Y.; He, H.; et al. Controlled Synthesis of Atomically Thin 1T-TaS2 for Tunable Charge Density Wave Phase Transitions. *Chem. Mater.* **2016**, *28* (21), 7613−7618.
(27) Wu, R. J.; Udyavara, S.; Ma, R.; Wang, Y.; Chhowalla, M.; Birol, T.; Koester, S. J.; Neurock, M.; Mkhoyan, K. A. Visualizing the Metal-MoS 2 Contacts in Two-Dimensional Field-Effect Transistors with Atomic Resolution. *Phys. Rev. Mater.* **2019**, *3*, 111001.
(28) Hirata, T.; Ohuchi, F. S. Temperature Dependence of the Raman Spectra of 1T-TaS2. *Solid State Commun.* **2001**, *117* (6), 361−364.
(29) Tison, Y.; Martinez, H.; Baraille, I.; Loudet, M.; Gonbeau, D. X-Ray Photoelectron Spectroscopy and Scanning Tunneling Microscopy Investigations of the Solid Solutions TixTa1-XS 2 ($0 \leq x \leq 1$). *Surf. Sci.* **2004**, *563* (1−3), 83−98.
(30) Zeng, Z.; Tan, C.; Huang, X.; Bao, S.; Zhang, H. Growth of Noble Metal Nanoparticles on Single- Layer TiS2 and TaS2 Nanosheets for Hydrogen Evolution Reaction. *Energy Environ. Sci.* **2014**, *7* (2), 797−803.
(31) *XPS Interpretation of Tantalum*. https://xpssimplified.com/elements/tantalum.php (accessed June 22, 2020).
(32) Kumar, A.; Akansel, S.; Stopfel, H.; Fazlali, M.; Åkerman, J.; Brucas, R.; Svedlindh, P. Spin Transfer Torque Ferromagnetic Resonance Induced Spin Pumping in the Fe/Pd Bilayer System. *Phys. Rev. B: Condens. Matter Mater. Phys.* **2017**, *95*, 064406.
(33) Liu, L.; Moriyama, T.; Ralph, D. C.; Buhrman, R. A. Spin-Torque Ferromagnetic Resonance Induced by the Spin Hall Effect. *Phys. Rev. Lett.* **2011**, *106* (3), 036601.
(34) Tserkovnyak, Y.; Brataas, A.; Bauer, G. E. W. Enhanced Gilbert Damping in Thin Ferromagnetic Films. *Phys. Rev. Lett.* **2002**, *88* (11), 117601.
(35) Demasius, K. U.; Phung, T.; Zhang, W.; Hughes, B. P.; Yang, S. H.; Kellock, A.; Han, W.; Pushp, A.; Parkin, S. S. P. Enhanced Spin-Orbit Torques by Oxygen Incorporation in Tungsten Films. *Nat. Commun.* **2016**, *7*, 10644.
(36) Saitoh, E.; Ueda, M.; Miyajima, H.; Tatara, G. Conversion of Spin Current into Charge Current at Room Temperature: Inverse Spin-Hall Effect. *Appl. Phys. Lett.* **2006**, *88* (18), 182509.
(37) Zhao, B.; Khokhriakov, D.; Zhang, Y.; Fu, H.; Karpiak, B.; Hoque, A.; Xu, X.; Jiang, Y.; Yan, B.; Dash, S. P. Observation of Charge to Spin Conversion in Weyl Semimetal WTe 2 at Room Temperature. *Phys. Rev. Res.* **2020**, *2* (1), 013286.
(38) Xu, H.; Wei, J.; Zhou, H.; Feng, J.; Xu, T.; Du, H.; He, C.; Huang, Y.; Zhang, J.; Liu, Y.; Wu, H.-C.; Guo, C.; Wang, X.; Guang, Y.; Wei, H.; Peng, Y.; Jiang, W.; Yu, G.; Han, X.; et al. High Spin Hall Conductivity in Large-Area Type-II Dirac Semimetal PtTe 2. *Adv. Mater.* **2020**, *32*, 2000513.
(39) Zhu, L.; Sobotkiewich, K.; Ma, X.; Li, X.; Ralph, D. C.; Buhrman, R. A. Strong Damping-Like Spin-Orbit Torque and Tunable Dzyaloshinskii−Moriya Interaction Generated by Low-Resistivity Pd 1−x Pt x Alloys. *Adv. Funct. Mater.* **2019**, *29* (16), 1805822.
(40) Zimmermann, B.; Mavropoulos, P.; Heers, S.; Long, N. H.; Blügel, S.; Mokrousov, Y. Anisotropy of Spin Relaxation in Metals. *Phys. Rev. Lett.* **2012**, *109* (23), 236603.
(41) Long, N. H.; Mavropoulos, P.; Bauer, D. S. G.; Zimmermann, B.; Mokrousov, Y.; Blügel, S. Strong Spin-Orbit Fields and Dyakonov-Perel Spin Dephasing in Supported Metallic Films. *Phys. Rev. B: Condens. Matter Mater. Phys.* **2016**, *94* (18), No. 180406(R).
(42) Amin, V. P.; Stiles, M. D. Spin Transport at Interfaces with Spin-Orbit Coupling: Formalism. *Phys. Rev. B: Condens. Matter Mater. Phys.* **2016**, *94* (10), 104419.
(43) Amin, V. P.; Stiles, M. D. Spin Transport at Interfaces with Spin-Orbit Coupling: Phenomenology. *Phys. Rev. B: Condens. Matter Mater. Phys.* **2016**, *94* (10), 104420.
(44) Fan, X.; Wu, J.; Chen, Y.; Jerry, M. J.; Zhang, H.; Xiao, J. Q. Observation of the Nonlocal Spin-Orbital Effective Field. *Nat. Commun.* **2013**, *4*, 1799.
(45) Dc, M.; Grassi, R.; Chen, J. Y.; Jamali, M.; Reifsnyder Hickey, D.; Zhang, D.; Zhao, Z.; Li, H.; Quarterman, P.; Lv, Y.; et al. Room-Temperature High Spin−Orbit Torque Due to Quantum Confinement in Sputtered BixSe(1−x) Films. *Nat. Mater.* **2018**, *17* (9), 800−807.
(46) Kawaguchi, M.; Shimamura, K.; Fukami, S.; Matsukura, F.; Ohno, H.; Moriyama, T.; Chiba, D.; Ono, T. Current-Induced Effective Fields Detected by Magnetotrasport Measurements. *Appl. Phys. Express* **2013**, *6* (11), 113002.
(47) Kim, K. W.; Lee, K. J.; Sinova, J.; Lee, H. W.; Stiles, M. D. Spin-Orbit Torques from Interfacial Spin-Orbit Coupling for Various Interfaces. *Phys. Rev. B: Condens. Matter Mater. Phys.* **2017**, *96* (10), 104438.
(48) Zibouche, N.; Kuc, A.; Musfeldt, J.; Heine, T. Transition-Metal Dichalcogenides for Spintronic Applications. *Ann. Phys.* **2014**, *526* (9−10), 395−401.

https://dx.doi.org/10.1021/acs.nanolett.0c01955
Nano Lett. 2020, 20, 6372−6380

(49) Zhao, B.; Karpiak, B.; Khokhriakov, D.; Hoque, A. M.; Xu, X.; Jiang, Y.; Dash, S. P. *Edelstein Effect in Type-II Weyl Semimetal WTe2 up to Room Temperature*. 2019, 1910.06225, arXive. https://arxiv.org/abs/1910.06225 (accessed June 22, 2020).

NOTE ADDED AFTER ASAP PUBLICATION

Due to a production error, this paper was published on August 17, 2020, with the incorrect version of the Supporting Information. The corrected version was reposted on August 19, 2020.

https://dx.doi.org/10.1021/acs.nanolett.0c01955
Nano Lett. 2020, 20, 6372−6380